Inverterless High-Power Interior Permanent-Magnet Automotive Alternator

Wen L. Soong, *Member, IEEE,* and Nesimi Ertugrul, *Member, IEEE*

***Abstract*—This paper describes a high-power brushless interior permanent-magnet (PM) automotive alternator which does not use an inverter. The "inverterless" alternator is designed with a high back electromotive force voltage and high reactance, and acts as a constant current source over much of its wide constant power operating speed range. In this configuration, a switched-mode rectifier can be used to regulate the dc output voltage and current, which avoids the complexity and high cost of an inverter. An analysis of the modeling and performance of interior PM machines in this inverterless topology is described. Experimental results showing an outstanding constant power speed range are presented for a 6-kW concept demonstrator machine tested using a three-phase resistive load to simulate inverterless operation.**

***Index Terms*—Automotive alternators, field weakening, interior permanent-magnet (PM) machines, switched-mode rectifiers.**

I. Introduction

CONVENTIONAL car alternators are based on a three-phase (3-ph) Lundell-type wound-field synchronous alternator with a 3-ph rectifier [see Fig. 1(a)]. The output voltage is regulated by adjusting the field current. These alternators are simple and low in cost (production cost about US$75) [1]. They are, however, limited in output power to about 1–2 kW [see Fig. 2(a)] due to scalability and efficiency issues. Other limitations include low output power at idle speeds, high transient load-dump overvoltages (up to 80 V), and brush life.

A. High-Power Alternator Requirements

Proposed new features in cars, such as electromechanical valves and active suspension systems, will increase the auxiliary electric power consumption and, hence, require a higher power alternator. It is predicted that in the near future the electrical load on the alternator will increase to about 4–6 kW in luxury cars [2]. This is in parallel with the proposal for a new 42-V system voltage in cars.

An example output specification [1] for such a high-power alternator is 4 kW at idle (600 r/min engine speed) rising linearly to 6 kW at maximum speed (6000 r/min) as shown in Fig. 2(b). This represents a challenging 10 : 1 constant power speed range.

Paper IPCSD-04-026, presented at the 2003 Industry Applications Society Annual Meeting, Salt Lake City, UT, October 12–16, and approved for publication in the IEEE TRANSACTIONS ON INDUSTRY APPLICATIONS by the Electric Machines Committee of the IEEE Industry Applications Society. Manuscript submitted for review July 1, 2003 and released for publication April 9, 2004. This work was supported by a 2001 University of Adelaide Small Research Grant and by a 2003 Australian Research Council Discovery Project Grant.

The authors are with the Electrical and Electronic Engineering Department, University of Adelaide, Adelaide, SA 5005, Australia (e-mail: wen.soong@adelaide.edu.au; nesimi.ertugrul@adelaide.edu.au).

Digital Object Identifier 10.1109/TIA.2004.830773

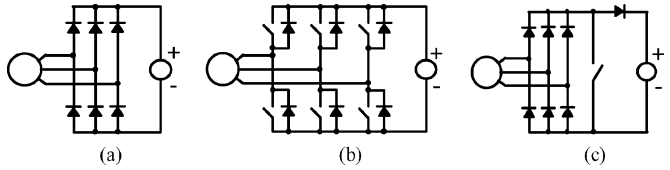

Fig. 1. (a) 3-ph rectifier. (b) Inverter drive. (c) Switched-mode rectifier.

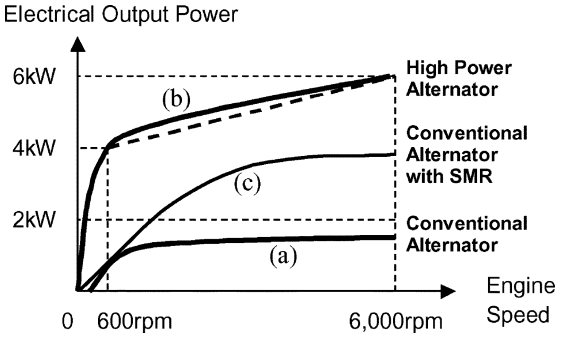

Fig. 2. Alternator output power versus engine speed. (a) Conventional alternator. (b) High-power alternator requirements. (c) Conventional alternator with switched-mode rectifier (SMR).

Other requirements include high system efficiency (at least 75% at 3-kW output at cruising speed of 1800 r/min), low system cost, a capability of safe overspeed operation to 10 000 r/min, and fast transient response to minimize load-dump overvoltages. If a starting function is also incorporated into the alternator, this should be capable of 150 N·m of starting torque.

B. Inverter-Driven Alternators

The majority of the present research work has focused on using a brushless inverter-driven machine [see Fig. 1(b)] acting as both a starter and a high-power alternator, producing the term "integrated starter/alternator" (ISA). An ISA represents an attractive stepping stone to a hybrid vehicle. Researchers have examined the implementation of an ISA using induction machines, switched reluctance machines, surface permanent-magnet (PM), and interior PM machines [1], [3]–[5].

The conventional alternator and starter have a total cost of approximately US$100. An inverter-driven ISA is considerably more expensive than this. This is largely due to the cost of the inverter which can exceed the cost of the machine by a factor of over 5 : 1. The estimated costs for an ISA system exceed US$500 [5]. The high cost of the inverter is associated with the number and ratings of the power electronic devices and their associated drivers, the complexity of high speed field-weakening control, and the need for position and current sensors (or sensorless algorithms).

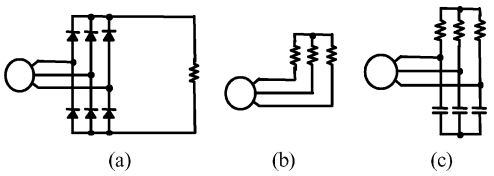

Fig. 3. Alternator with different output loads. (a) 3-ph rectifier/resistive load. (b) 3-ph resistive load. (c) 3-ph parallel resistive/capacitive load.

C. Switched-Mode Rectifiers With Conventional Alternators

For alternators based on PM machines it is possible to use a 3-ph switched-mode (or boost) rectifier [see Fig. 1(c)], instead of an inverter. This has been used with surface PM machines to produce a regulated output voltage which is greater than the back electromotive force (EMF) voltage [6]. This topology makes use of the small leakage reactance of the surface PM machine to avoid the necessity for an external inductor.

Perreault [7], [8] has proposed a means for increasing the available output power from a conventional Lundell alternator by using a switched-mode rectifier to allow the alternator to operate at its maximum output power point over a wide range of speeds and yet still deliver a constant output voltage. Note that conventional alternators have high synchronous reactances and that the output voltage from the switched-mode rectifier in this case can be either higher or lower than the back-EMF voltage.

Perreault's results show a substantial output power improvement at higher speeds [see Fig. 2(c)] compared with the conventional rectifier, though it falls short of the high-power alternator requirements. Despite this, his proposal is attractive as a low-cost means for obtaining more output power from conventional alternators. However, there are still remaining issues, with limitations on the brushes, power output at idle speeds, and the system efficiency.

D. Uncontrolled Generation

The proposed inverterless approach utilizes what was previously considered a fault mode of inverter-driven PM machines called uncontrolled generation.

Consider an inverter-driven PM machine [see Fig. 1(b)] operating as a motor at high speed where the induced back-EMF voltages exceed the supply voltage. A controller fault occurs which disables the inverter switches, leaving only the freewheeling diodes [see Fig. 1(a)]. The high back-EMF voltages now cause the machine to act as a generator.

This situation is normally undesirable as the resultant high generating currents could damage the machine or cause system overvoltages if the dc bus is unable to absorb the regenerated power. For this reason, it is considered desirable that the back-EMF voltage of PM machines at maximum speed be kept lower than the rated output voltage [9].

Uncontrolled generation was described initially by Adnanes [10]. Later, Jahns *et al.* [9], [11] performed a detailed study of this effect. They showed that for analysis purposes, the dc voltage source in Fig. 1(a) could be approximated as a resistive load [see Fig. 3(a)] and the configuration further simplified to a 3-ph resistive load [see Fig. 3(b)].

E. Inverterless Concept

The inverterless concept arose from research into means for testing the field-weakening generating performance of interior PM machines without an inverter. In an inverter-driven PM generator, the inverter effectively acts as a variable load impedance (normally with leading power factor). Thus, at a particular speed and generating load, the inverter can be replaced by a passive load with the same equivalent resistance and capacitance [see Fig. 3(c)]. Removing the capacitors yields the 3-ph resistive load in Fig. 3(b) which Jahns has shown to be equivalent to uncontrolled generation.

The proposed inverterless concept is based on operating an optimized interior PM machine with the switched-mode rectifier arrangement used by Perreault. This avoids the complexity and high cost of an inverter. It also eliminates the need for a position sensor, minimizes the power electronic switch VA ratings, and has simple control requirements. Note that in the inverterless arrangement, ideally the switch will not see any more than the rated dc output voltage and current.

The machine costs for the inverterless arrangement should be comparable to inverter-driven machines; however, the cost of the power electronics and control circuitry should be much lower than for an inverter. Hence, the cost of an inverterless system is expected to be closer to the conventional alternator than to the inverter solution. The inverterless concept is thus attractive as a low-cost stepping stone to produce a higher power alternator for conventional cars.

Note that the inverterless interior PM machine cannot act as a motor and, hence, would still require the conventional starter motor (estimated cost US$25 [1]).

II. Inverterless Operation of Interior PM Machines

An analysis of the performance and optimization of inverterless interior PM machines is described in this section.

A. Alternator Characteristics With Resistive Load

Based on the discussion in the previous section, a convenient first step is to examine the performance of interior PM machines with a 3-ph resistive load. The output current and power versus output voltage loci can be obtained by solving the interior PM machine's steady-state equations for a variable resistive load [9], [12]. Assuming a lossless, magnetically linear model, it can be shown that when these curves are normalized to the machine's short-circuit current and open-circuit voltage, their shape is not affected by speed and depend only on the machine's saliency ratio (see Fig. 4).

For a saliency ratio of unity, that is, a surface PM machine, the machine equivalent circuit corresponds to a voltage source with a series reactance. With a resistive load, this yields the semicircular output current–voltage locus shown in Fig. 4. Maximum power occurs with an output current of about 70% of the short-circuit current. Note that as the saliency ratio is increased from unity, the maximum output power increases significantly.

For saliency ratios exceeding two, the curve develops an increasing voltage overshoot, that is, the output voltage under load can be higher than the open-circuit voltage. For instance, with

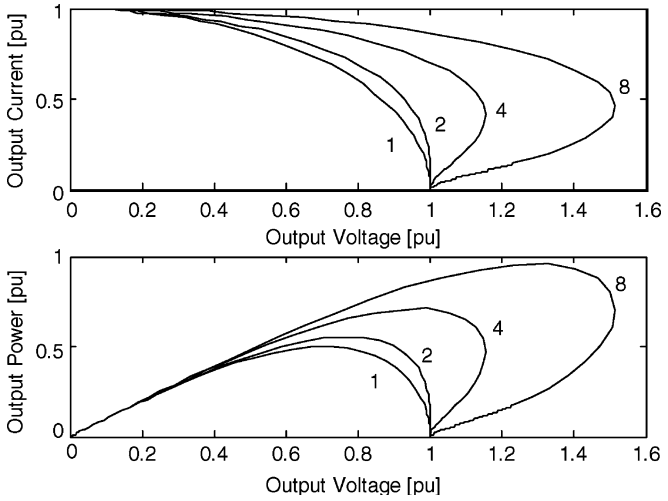

Fig. 4. Ideal normalized current and power versus voltage loci for interior PM machines with a 3-ph resistive load for saliency ratios of 1, 2, 4, and 8.

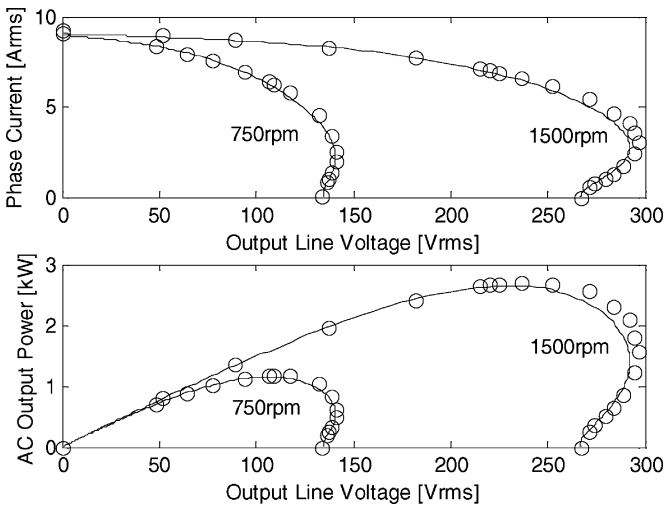

Fig. 5. Plot of current and power versus voltage curves for the concept demonstrator machine at two speeds with a 3-ph resistive load. Calculated results (lines) and experimental results (circles).

a saliency ratio of 8, at an output current of 0.5 pu, the output voltage is about 50% higher than the open-circuit voltage. This characteristic is responsible for the bistable or hysteresis effect during uncontrolled generation which was observed by Jahns [9]. For saliency ratios below 0.5 (not shown), a current overshoot occurs where the output current under load can exceed the short-circuit current.

Fig. 5 shows a good correspondence between the calculated and measured characteristics of the concept demonstrator interior PM alternator (described in Section III) with a 3-ph resistive load at two speeds. This machine has an unsaturated saliency ratio of approximately 6. The calculated curve includes the effect of stator resistance and magnetic saturation, which has reduced the predicted voltage overshoot to about 10% compared with over 30% which was expected from interpolating the curves in Fig. 4. This reduction is largely due to the heavy magnetic saturation in this alternator (see Fig. 9).

It is interesting to consider how the shape of the current–voltage loci shown in Fig. 5 varies with speed. The PM flux causes the open-circuit voltage to be proportional to speed. As the machine reactances are also proportional to speed, the short-circuit current should, thus, be independent of speed (ignoring stator resistance). If the back-EMF voltage is large compared with the output voltage, then the output current will not be significantly affected by speed and the alternator acts like a constant current source. Thus, with a constant load resistance, the output voltage will be relatively independent of speed. This is an important point as it allows the machine to deliver constant output current and voltage (hence, power) over a wide speed range. Adding a rectifier converts the 3-ph ac output into dc. An additional switch and diode produces the switched-mode rectifier shown in Fig. 1(c) which allows regulation of the output voltage.

Note that this constant current characteristic is opposite to "traditional" PM generators which normally act as voltage sources whose output voltage is proportional to speed.

The switched-mode rectifier has two modes of operation. At low speeds, the back-EMF voltage is lower than the output voltage and the switched-mode rectifier acts as a form of boost rectifier. At high speeds, the machine acts as a constant current source and the duty cycle of the switch controls the output current.

In order to fully utilize this constant current characteristic, the machine should be designed with a back-EMF voltage which is much larger than the rated output voltage, and a short-circuit current which is equal to the rated output current. Consequently, the machine should have both high back-EMF voltage and high reactance. This is similar to the characteristics of the conventional Lundell alternator used by Perreault. Note that making the short-circuit current equal to the rated current has been shown to give the best field-weakening performance in PM machines [13], [14].

B. Normalization Procedure

The effect of the choice of the interior PM machine parameters on the output power versus speed characteristics under both inverter and inverterless operation will now be examined. A lossless, linear model will again be used and only machine designs where the short-circuit current is equal to rated current will be considered (henceforth referred to as optimal designs). In other words, it is assumed that the magnet stator flux linkage Ψ_m and the d-axis inductance L_d will be chosen so that $\Psi_m = L_d I_0$ where I_0 is the rated current.

The two design parameters for optimal interior PM machines which will be used in this analysis are the saliency ratio $\xi = L_q/L_d$ (where L_q is the q-axis inductance), and the back-EMF ratio $\kappa = E/V_0$. The back-EMF ratio is the ratio of the back-EMF voltage $E = \Psi_m \omega$ at the rated speed ω_0, to the rated voltage V_0. In previous work [13], the rated speed was chosen to be the highest speed at which rated torque could be produced; however, in this paper the rated speed will be chosen to be the maximum speed in the constant power speed range (CPSR).

Applying the above normalization yields the normalized magnet flux linkage $\Psi_{mn} = \kappa$, normalized d-axis inductance $L_{dn} = \kappa$ and normalized q-axis inductance $L_{qn} = \xi\kappa$. It will be assumed that the rated machine output voltage and current cannot be exceeded. Using these results, the output power characteristics of optimal interior PM machines can

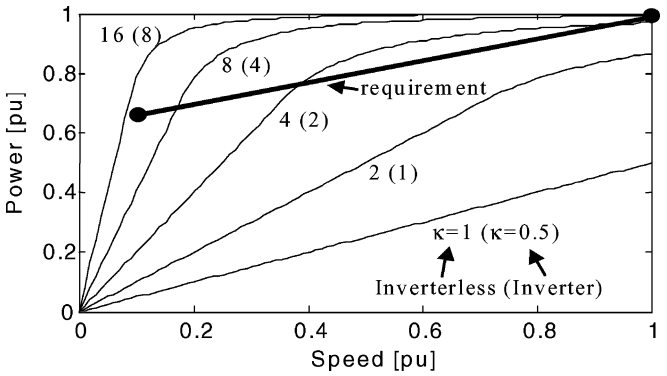

Fig. 6. Output power versus speed characteristics for optimal surface PM alternators as a function of the back-EMF ratio κ, under inverterless operation. The corresponding back-EMF ratio for inverter operation is shown in brackets. The high-power alternator requirement is also indicated.

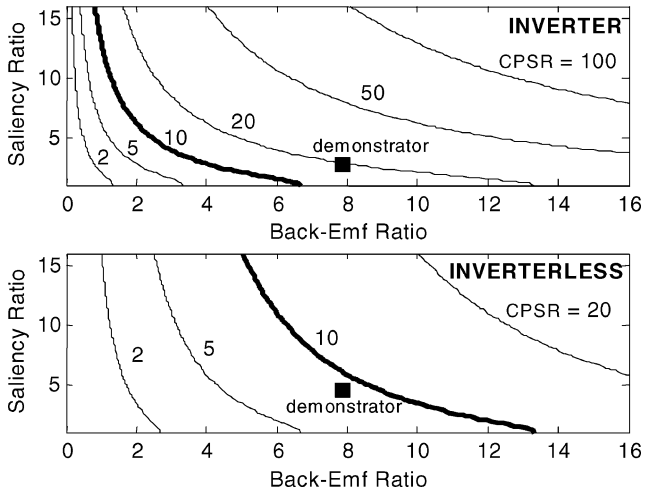

Fig. 7. CPSR contour plots for optimal interior PM machines as a function of back-EMF ratio and saliency ratio, for inverter and inverterless operation. The high-power alternator requirement of a CPSR of 10 is highlighted. The location of the concept demonstrator design is shown.

now be calculated using the approach given in [13] for inverter operation and in [9], [10], and [12] for inverterless operation.

C. Optimal Surface PM Machines

Fig. 6 shows the normalized output power versus speed characteristics of surface PM machines (i.e., $\xi = 1$) for various back-EMF ratios κ for both inverterless and inverter operation.

The electrical power versus speed curves initially linearly increase (representing constant input torque) up to an output power of about 0.7 pu, and then asymptote toward 1 pu for higher speeds. The shape of all the curves are identical and hence each curve can be defined by only its initial slope. This initial slope is the maximum input torque capability of the alternator at rated current, and is linearly proportional to the back-EMF ratio κ (that is, the magnet flux).

For a surface PM alternator of a given back-EMF ratio, it can be shown that the maximum input torque under inverter operation is twice that achievable under inverterless operation. This is because of the greater control flexibility available with inverter operation. Thus the output curve for inverterless operation at a back-EMF ratio of 16 corresponds to the curve for inverter operation with a back-EMF ratio of 8.

The high power alternator requirement is 4 kW at 600 r/min linearly increasing to 6 kW at 6000 r/min. Normalizing this gives a requirement of 2/3 pu output power at 0.1 pu speed increasing to 1 pu output power at 1 pu speed. To achieve this, from Fig. 6 it can be shown that an inverter-driven surface PM machine requires a high back-EMF ratio of 6.67 while the inverterless configuration requires a back-EMF ratio of 13.33.

D. Optimal Interior PM Machines

With the high-power alternator requirement in mind, it is convenient to define the CPSR of an interior PM alternator as the speed range over which the output power is greater than 2/3 pu. Thus, the high-power alternator requirement is a CPSR of 10. As 2/3 pu output power corresponds to operation in the constant input torque region (i.e., less than about 0.7 pu output power), then the CPSR can be found from the maximum input torque. For inverter operation, the maximum input torque corresponds to operation at the maximum torque per ampere point [13]. For inverterless operation, the maximum input torque can be found by differentiating the relation given in [12] relating the input torque to the value of load resistance.

Fig. 7 shows contour plots of the CPSR for optimal interior PM machines as a function of the back-EMF ratio and the saliency ratio for both inverter and inverterless operation. The x axis corresponds to a saliency ratio of unity (surface PM alternators) which was considered in Fig. 6. Note that for surface PM machines, the CPSR for inverter operation is twice that for inverterless operation.

For a given back-EMF ratio, increasing the saliency ratio significantly improves the CPSR; however, the improvement is much greater for inverter than for inverterless operation.

Note that to achieve a CPSR of 10 with an inverter-driven machine, the normal design requirement to keep the back EMF at maximum speed at less than the rated voltage [9] (i.e., back-EMF ratio $\kappa < 1$) would require a very high saliency ratio of about 13.

The location of the concept demonstrator design is shown as a square in Fig. 7 using the measured back-EMF ratio of 7.8, and calculated saturated saliency ratios of 2.7 for inverter operation and 4.6 for inverterless operation (from the measured flux-linkage curves in Fig. 9). Experimental results for this machine are presented in the next section.

III. Concept Demonstrator Machine

Earlier, the authors constructed a multiple-barrier interior PM rotor (see Fig. 8) for a commercial four-pole 2.2-kW 415-V 50-Hz induction machine stator. The rotor was initially tested with ferrite magnets and the results reported in [12] and [15]. These have now been replaced with rare-earth (NdFeB) magnets to increase the magnet flux. Though this machine was not specifically designed for this purpose, it provides a useful concept demonstrator for a belt-driven (3 : 1 ratio) high-power automotive alternator. Note that though the voltage rating of this machine is much larger than the alternator requirement, rewinding it for a lower voltage (and, hence, higher current) will not change its output power or efficiency characteristics.

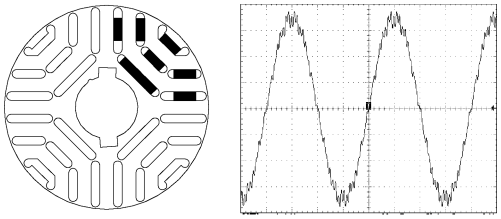

Fig. 8. Rotor lamination cross section with ferrite magnets (left) and measured line back-EMF waveform at 1500 r/min with NdFeB magnets (right). The line voltage is 271 Vrms.

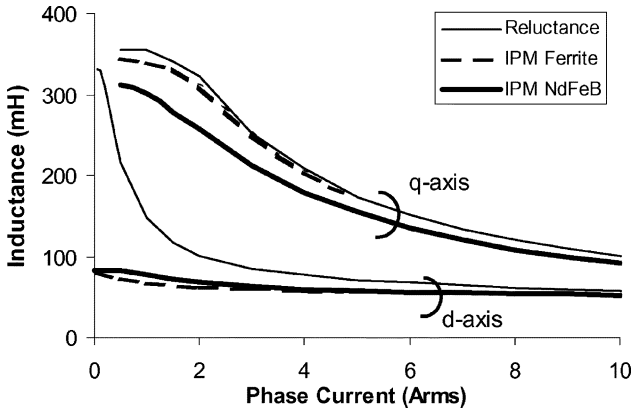

Fig. 9. Measured d-axis and q-axis inductance saturation curves for the machine without magnets, with ferrite magnets, and with NdFeB magnets.

A. Parameter Measurement

The measured inductance saturation parameters of the machine are shown in Fig. 9 for the machine without magnets (reluctance), with ferrite magnets and then with NdFeB magnets. The induction machine stator was rated at 4.8 A and the inductances have been measured at currents up to twice this value. This causes heavy saturation in the q-axis of the machine. The addition of magnet flux in the d-axis produces a cross-saturation effect which reduces the q-axis inductance. This is relatively small with ferrite magnets but significant with NdFeB magnets.

The d-axis curves are strongly affected by saturation of rotor bridges (see Fig. 8) when no magnets are present. In the PM machines, the magnet flux saturates the rotor bridges and so produces a relatively constant d-axis inductance.

Fig. 8 also shows the measured back-EMF waveform of the machine with NdFeB magnets. Assuming a maximum speed of 18 kr/min with a 3 : 1 belt ratio, this gives a very high back-EMF ratio of nearly 8 (see Table I).

Table I also shows the measured high-speed short-circuit current of the PM machines, the maximum saliency ratio (calculated as the unsaturated value of L_q divided by the saturated value of L_d), and the ideal maximum inverterless output power calculated from the rated voltage (415 V) and the short-circuit current.

B. Mechanical Strength

A key limitation of the concept demonstrator machine is the mechanical strength of the rotor. The high power alternator specification, assuming a 3 : 1 belt ratio, requires a rated alternator maximum speed of 18 kr/min and an overspeed capability of 30 kr/min [1].

The failure speed of the concept demonstrator has been roughly estimated to be in the order of 12–15 kr/min. This could be improved by optimising the location, number and thickness of the rotor ribs [16] and by carefully selecting the heat treatment of the laminations to trade off magnetic properties for improved mechanical strength [17]. Increasing the thickness or number of the rotor ribs will increase the magnet leakage flux and will require more permanent magnet material in the rotor to achieve the same back EMF. Note that the rotor cross section in Fig. 8 shows there is significant room in the rotor to add more PM material.

TABLE I
COMPARISON OF ROTORS IN 415 V 2.2 kW INDUCTION MOTOR STATOR

	Reluctance	IPM Ferrite	IPM NdFeB
Line Back-EMF at 1,500rpm	0	83V	271V
Short-Circuit Current	0	2.2A	9.3A
Back-EMF at 18krpm	0	1.0kV	3.25kV
Back-EMF ratio κ at 18krpm	0	2.4	7.8
Max Saliency Ratio ξ	3.3	6.1	5.7
Inverterless Output Power	0	≈1.6kW	≈6.9kW

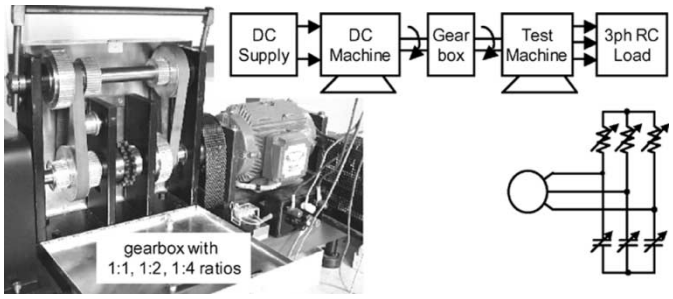

Fig. 10. Block diagram of experimental setup, photograph of the gearbox and concept demonstrator machine, and the circuit for the 3-ph variable resistive/capacitive load.

C. Dynamometer Arrangement

The interior PM concept demonstrator was driven by two 5-kW 1500-r/min dc machines through a belt drive with adjustable gear ratios of 1 : 1, 1 : 2, and 1 : 4 which gave a maximum speed of 6000 r/min (see Fig. 10). A 220-V/50-A variable dc power supply was used to drive the dc machines. The reaction torque on the alternator stator was measured using a load cell.

The three different load configurations shown in Fig. 3 were produced using combinations of a 3-ph rectifier, three 240-V/20-A single-phase variable resistance banks and a 3-ph 440-V/120-μF variable capacitance bank. The capacitance bank could be connected in star (to give a range of 0–120 μF, 0.5-μF steps) or delta (to give a range of 0–360 μF, 1.5-μF steps). Higher capacitance values were achieved by adding external fixed capacitor banks.

Fig. 11 shows the calculated resistance/capacitance values used to simulate inverter operation, in order to obtain the results shown in Fig. 14.

IV. EXPERIMENTAL TEST RESULTS AND DISCUSSION

In this section the performance of the interior PM concept demonstrator under both inverter and inverterless operation is examined. As neither an inverter nor a switched-mode rectifier

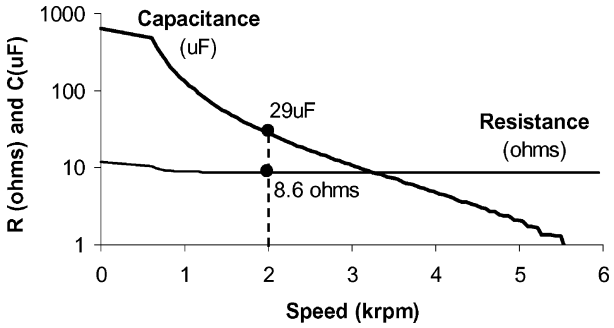

Fig. 11. Calculated 3-ph parallel resistance and capacitance per phase used to produce the "inverter" maximum output power characteristics in Fig. 14. For example, at 2 kr/min, a resistance of 8.6 Ω and capacitance of 29 μF are required.

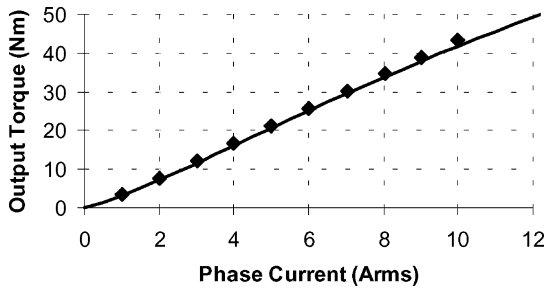

Fig. 12. Concept demonstrator torque versus current characteristic. Calculated characteristic based on the measured machine parameters (solid line) and measured generating torque with 3-ph *RC* load (diamonds).

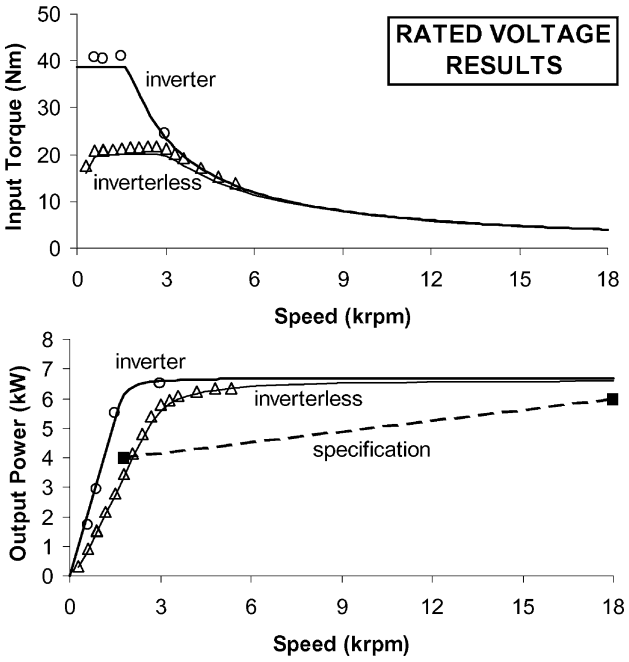

Fig. 13. Torque and power versus alternator speed curves at rated voltage showing the measurements under "inverter" (circles) and "inverterless" (triangles) operation, the calculated curves (lines), and the alternator specification.

was available during the testing, inverter operation was simulated with a 3-ph parallel resistive/capacitive load and inverterless operation was simulated with a 3-ph resistive load.

A. Inverter-Driven Starting Torque Performance

The engine starting torque requirement is 150 N·m. With a 3 : 1 belt drive this would be equivalent to 50 N·m at the starter/alternator.

Fig. 12 shows the torque versus current characteristic with a 3-ph resistive/capacitive load simulating an inverter. The generating torque measurements show a close correspondence to the calculations. The measurements are slightly higher due to iron and windage/friction losses which were not modeled in the calculations. Note that apart from these losses, the motoring and generating torque versus current characteristics should be identical. The results indicate that the required 50-N·m starting torque should be achievable with an inverter current of about 12 A.

B. Generating Output With 3-ph Resistive and Resistive/Capacitive Loads

The concept demonstrator alternator was tested using a 3-ph resistive load to simulate inverterless operation and a 3-ph resistive/capacitive load to simulate inverter operation at alternator speeds of up to 6000 r/min (corresponding to an engine speed of 2000 r/min). The rated current under inverter operation was chosen to be equal to the alternator short-circuit current (9.3 A).

Tests were performed at rated line voltage (415 V) to verify the low-speed output power capability (see Fig. 13). However, the 6000 r/min dynamometer speed restriction meant that the expected 10 : 1 CPSR could not be demonstrated. Thus, further tests at one-third rated line voltage were necessary to verify the CPSR (see Fig. 14).

The calculated results shown in Figs. 13 and 14 used the measured interior PM machine parameters and included the effect of stator resistance and magnetic saturation but not iron or friction/windage losses.

The measured output power under both inverter and inverterless operation shows an excellent correspondence with the calculations. The measured input torque is slightly higher than predicted due to iron and friction/windage losses which were not modeled.

Fig. 13 shows that the concept demonstrator easily meets the idle power requirement associated with the 10 : 1 CPSR specification under inverter operation, and nearly meets it under inverterless operation. These results correspond well with the location of its design parameters on the CPSR contour plots shown in Fig. 7. Note that at low speeds, the output power under inverter operation is about twice that under inverterless operation but that they asymptote to the same value at high speeds.

In Fig. 14 the machine was tested at one-third rated voltage in order to demonstrate its CPSR. A one-third scaled specification is shown for reference. Even with the loss of performance at the lower voltage due to the more pronounced effect of stator resistance, the machine demonstrates an outstanding CPSR which exceeds the 10 : 1 specification under inverter operation and is close to meeting it under inverterless operation. The drop in the inverterless input torque (and hence output power) at very low speeds is due to stator resistance.

C. Losses and Efficiency

Fig. 15 shows the measured losses as a function of speed for the inverterless (resistive load) operation corresponding to the

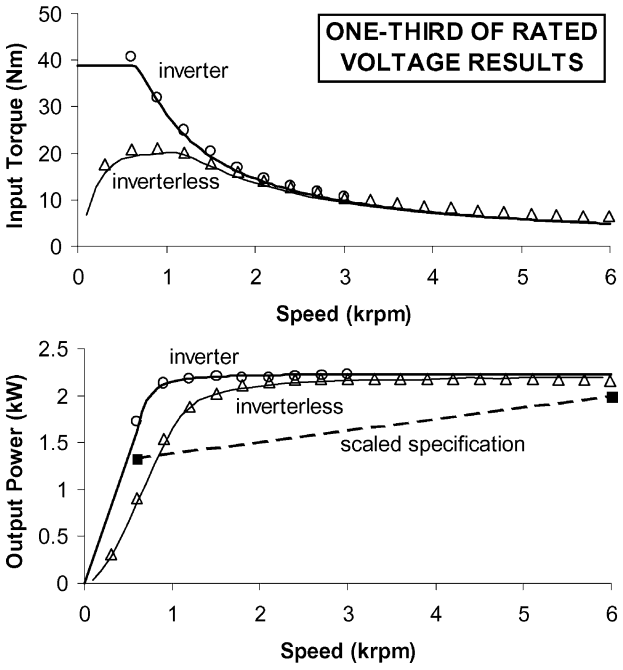

Fig. 14. Torque and power versus alternator speed curves at one-third of rated voltage showing the measurements under "inverter" (circles) and "inverterless" (triangles) operation, the calculated curves (lines), and the "scaled" alternator specification.

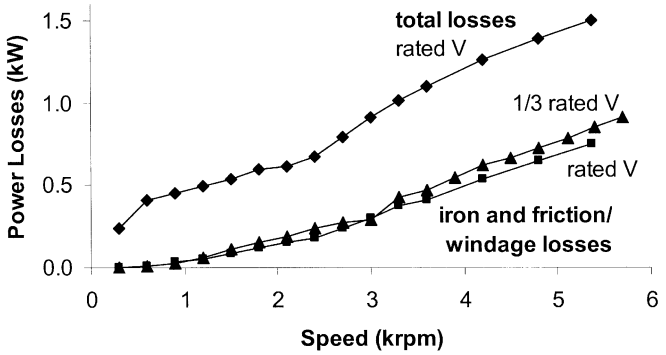

Fig. 15. Measured losses under "inverterless" operation for the concept demonstrator. The total losses are shown at rated voltage. The iron and friction/windage losses are shown at both rated and one-third rated voltage.

output power versus speed curves in Figs. 13 and 14. It shows both the total losses and the losses after stator copper losses are removed leaving the friction/windage and iron losses.

The iron and friction/windage losses show an approximately square law relationship with speed. At 6 kr/min they are roughly equal to the stator copper losses. This result is a major concern for a machine which is required to operate up to 18 kr/min. As the outside of the rotor is smooth, the windage losses should be relatively low. It is, therefore, assumed that the majority of these losses are iron losses.

The high iron losses are likely to be due to the high flux densities in the machine associated with the high back-EMF voltage. Though the stator currents reduce the fundamental component of the air-gap magnetic field in the machine at high speeds, significant harmonic components may still be present which could cause large losses. This is consistent with Fig. 15 which shows the losses are not significantly affected by the output voltage.

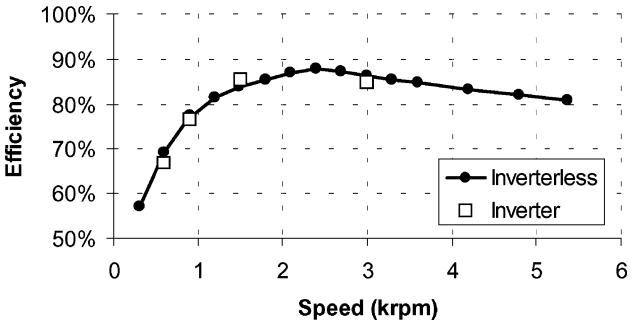

Fig. 16. Measured efficiency at rated voltage of the concept demonstrator corresponding to the power output curves shown in Fig. 13.

The losses could be reduced by means such as : lowering the required back-EMF voltage by optimizing the machine to improve its saliency ratio (see Fig. 7); redesigning the machine to reduce the harmonic flux components; and using thinner and lower loss lamination material [17].

Note that the measured electrical output power in the one-third rated voltage test (Fig. 14) is close to the calculated values despite nearly 1 kW of unmodeled iron and friction/windage losses. It thus appears that these losses increase the required mechanical input power but do not significantly affect the electrical output power.

Fig. 16 shows the measured efficiency of the alternator at the full-load, rated voltage conditions shown in Fig. 13 for both inverter and inverterless operation. The efficiency at a given speed under the two modes of operation is surprisingly similar despite the considerable difference in output power between them, particularly at lower speeds. At higher speeds the efficiency was expected to remain constant. The measured fall in efficiency is due to the high iron losses shown in Fig. 15.

D. Generating With Diode Rectifier/Voltage Source

The alternator was also tested while operating through a diode rectifier into a dc voltage source [see Fig. 1(a)]. The waveforms in Fig. 17 show operation at both low and high speeds. It is interesting to observe that they resemble the waveforms in brushless PM motors when driven from a six-step inverter. The waveforms correspond well to those observed earlier by Adnanes [10].

E. Generating With Diode Rectifier/Resistive Load

The "inverterless" operation output power tests in Figs. 13 and 14 used a 3-ph resistive load to simulate the switched-mode rectifier. To give greater confidence in the results, the alternator output power characteristics when operating through a diode rectifier into a resistive load [see Fig. 3(a)] was measured. Fig. 18 shows both the machine ac output and the rectifier dc output characteristics. Note that the equivalent ac output voltage for a given dc output voltage was calculated from the fundamental component of the ideal six-step voltage waveform shown in Fig. 17.

The results confirm that the machine is capable of delivering the required 6 kW dc output power. The ac characteristics closely follow the calculated curves while the dc characteristics show some significant deviations at low currents where the current waveform is discontinuous. The dc output voltage rises

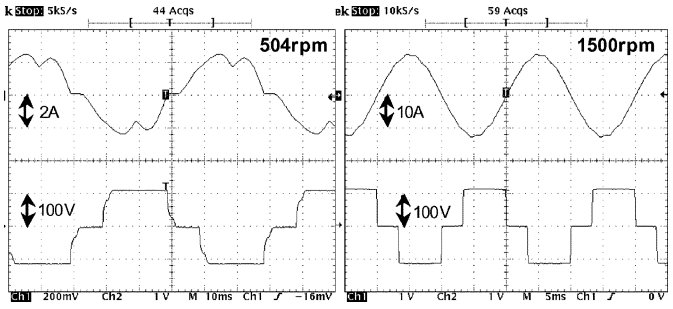

Fig. 17. Measured generating waveforms with the alternator operating through a diode rectifier into a 110-V dc voltage source at low and high speeds. Alternator phase current (upper) and line voltage (lower).

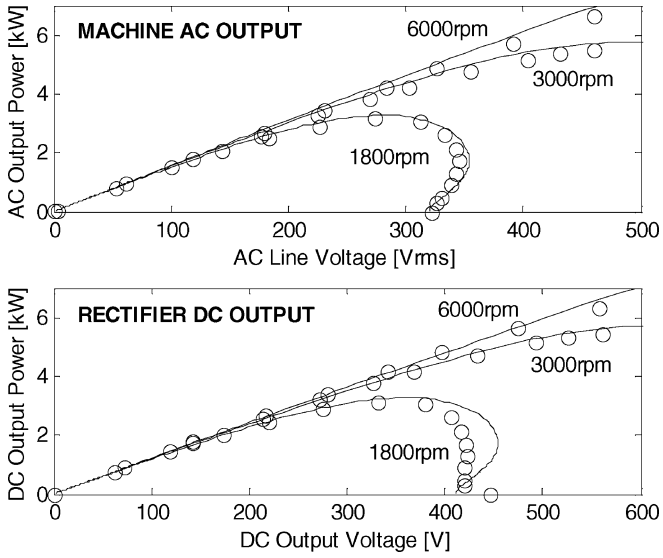

Fig. 18. Concept demonstrator performance when driving a resistive load through a rectifier. Top graph shows the machine ac output power versus ac line voltage and lower graph shows the rectifier dc output power versus dc output voltage. Measured (circles) and calculated (solid lines).

unexpectedly on open circuit, possibly due to the harmonics in the open-circuit voltage (see Fig. 8).

V. Conclusion

This paper has proposed a low-cost means of implementing a 6-kW interior PM automotive alternator with a wide CPSR using a switched-mode rectifier instead of an inverter. This was referred to as inverterless operation. The optimum design and analysis of interior PM machines for inverterless operation was discussed and preliminary results for a concept demonstrator machine using a 3-ph resistive load to simulate the switched-mode rectifier were presented. The key results of this paper are as follows.

- A high-back-EMF, high-reactance PM alternator can efficiently deliver constant power with a constant output voltage over a wide speed range.
- The optimum design for wide CPSR operation for inverterless (and inverter-driven) PM alternators is to choose the magnet flux and d-axis inductance such that the short-circuit current is equal to the rated output current.
- For optimal interior PM alternator designs, the CPSR is determined by two parameters: the back-EMF ratio (the ratio of the back-EMF voltage at maximum speed to the rated output voltage), and the saliency ratio.
- Inverterless operation gives lower output power at low speeds than inverter operation (and, hence, poorer CPSR) but similar high-speed output power.
- For a given CPSR with an optimal interior PM machine, increasing the saliency ratio reduces the required value of the back-EMF ratio; however, the effect is much larger for inverter operation than for inverterless operation.
- An extensive series of tests on an interior PM concept demonstrator machine has validated the theoretical results and it was demonstrated, using a 3-ph resistive load to simulate inverterless operation, that this machine can deliver over 6 kW and that it has an extremely wide CPSR.

In summary, it has been shown that a high-back-EMF, high-reactance interior PM alternator with a switched-mode rectifier has potential as a low-cost alternative to an inverter drive for applications such as high-power automotive alternators.

Areas for further work include: demonstrating steady-state and dynamic operation using a switched-mode rectifier, redesigning the machine to reduce the very high iron losses and to improve the rotor mechanical speed capability, adding an auxiliary switch to prevent overvoltages under fault conditions, and finally demonstrating operation on a car engine.

Acknowledgment

The authors thank the staff of the School of Electrical and Electronic Engineering's mechanical workshop for construction of the rotor and dynamometer and to C. Z. Liaw for support in the testing. They also gratefully acknowledge technical discussions with E. C. Lovelace, T. M. Jahns, and B. A. Welchko.

References

[1] E. C. Lovelace, "Optimization of a magnetically saturable interior permanent-magnet synchronous machine drive," Ph.D. dissertation, Dept. Elect. Eng. Comput. Sci., Massachusetts Inst. Technol., Cambridge, MA, 2000.

[2] J. G. Kassakian, J. M. Miller, and N. Traub, "Automotive electronics power up," *IEEE Spectr.*, vol. 37, pp. 34–39, May 2000.

[3] J. M. Miller, A. R. Gale, P. J. McCleer, F. Leonardi, and J. H. Lang, "Starter-alternator for hybrid electric vehicle: Comparison of induction and variable reluctance machines and drives," in *Conf. Rec. IEEE-IAS Annu. Meeting*, 1998, pp. 513–523.

[4] F. Caricchi, F. Crescimbini, E. Santini, and L. Solero, "High-efficiency low-volume, starter/alternator for automotive applications," in *Conf. Rec. IEEE-IAS Annu. Meeting*, 2000, pp. 215–222.

[5] E. C. Lovelace, T. M. Jahns, J. L. Kirtley, and J. H. Lang, "An interior PM starter alternator for automotive applications," in *Conf. Rec. IEEE IEMDC'98*, vol. 3, 1998, pp. 1802–1808.

[6] G. Venkataramanan, B. Milkovska, V. Gerez, and H. Nehrir, "Variable speed operation of permanent magnet alternator wind turbines using a single switch converter," *J. Solar Energy Eng.*, vol. 118, pp. 235–238, Nov. 1996.

[7] D. J. Perreault and V. Caliskan, "Automotive power generation and control," Massachusetts Inst. Technol., Cambridge, MA, LEES Tech. Rep. TR-00-003, May 2000.

[8] ——, "A new design for automotive alternators," presented at the IEEE SAE Int. Conf. Transportation Electronics (Convergence), Detroit, MI, Oct. 2000, SAE Paper 2000-01-C084.

[9] T. M. Jahns and V. Caliskan, "Uncontrolled generator operation of interior PM synchronous machines following high-speed inverter shutdown," *IEEE Trans. Ind. Applicat.*, vol. 35, pp. 1347–1357, Nov./Dec. 1999.

[10] A. K. Adnanes, R. Nilssen, and R. O. Rad, "Power feed-back during controller failure in inverter fed permanent magnet synchronous motor drives with flux-weakening," in *Proc. IEEE PESC'92*, 1992, pp. 958–963.

[11] V. Caliskan, D. J. Perreault, T. M. Jahns, and J. G. Kassakian, "Analysis of three-phase rectifiers with constant-voltage loads," in *Proc. IEEE PESC'99*, 1999, pp. 715–720.

[12] B. A. Welchko, T. M. Jahns, W. L. Soong, and J. M. Nagashima, "IPM synchronous machine drive response to symmetrical and asymmetrical short circuit faults," *IEEE Trans. Energy Conversion*, vol. 18, pp. 291–298, June 2003.

[13] W. L. Soong, "Design and modeling of axially-laminated interior permanent magnet motor drives for field-weakening applications," Ph.D. dissertation, Dept. Electron. Elect. Eng., Univ. Glasgow, Glasgow, U.K., 1993.

[14] W. L. Soong and T. J. E. Miller, "Field-weakening performance of the five classes of brushless synchronous AC motor drives," *Proc. IEE—Elect. Power Applicat.*, vol. 141, no. 6, pp. 331–340, Nov. 1994.

[15] W. L. Soong, N. Ertugrul, E. C. Lovelace, and T. M. Jahns, "Investigation of interior permanent magnet offset-coupled automotive integrated starter/alternator," in *Conf. Rec. IEEE-IAS Annu. Meeting*, 2001, pp. 429–436.

[16] E. C. Lovelace, T. M. Jahns, T. A. Keim, and J. H. Lang, "Mechanical design considerations for conventionally-laminated, high-speed interior PM synchronous machine rotors," in *Conf. Rec. IEEE IEMDC'01*, 2001, pp. 163–169.

[17] W. L. Soong, G. B. Kliman, R. N. Johnson, R. White, and J. Miller, "Novel high speed induction motor for a commercial centrifugal compressor," *IEEE Trans. Ind. Applicat.*, vol. 36, pp. 706–713, May/June 2000.

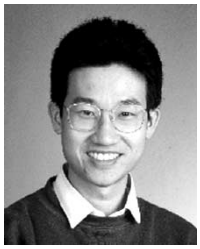

Wen L. Soong (S'89–M'90) was born in Kuala Lumpur, Malaysia. He received the B.Eng. degree from the University of Adelaide, Adelaide, Australia, in 1989, and the Ph.D. degree from the University of Glasgow, Glasgow, U.K., in 1993.

He was an Electrical Engineer for four years in the Power Controls Program at General Electric Corporate Research and Development, Schenectady, NY, before taking up a teaching position in the Electrical and Electronic Engineering Department, University of Adelaide, in 1998. His present research interests include permanent-magnet and reluctance machines, renewable energy generation, magnetic levitation, and condition monitoring and diagnostics.

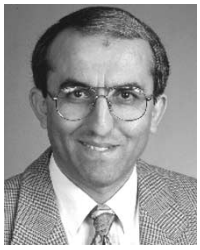

Nesimi Ertugrul (M'95) received the B.Sc. and M.Sc. degrees in electrical and electronic and communication engineering from Istanbul Technical University, Istanbul, Turkey, in 1985 and 1989, respectively, and the Ph.D. degree from the University of Newcastle-upon-Tyne, Newcastle-upon-Tyne, U.K., in 1993.

Since 1994, he has been with Adelaide University, Adelaide, Australia, where he is a Senior Lecturer. His primary research topics include sensorless operation of switched motors, fault-tolerant motor drives, condition monitoring, and electric vehicles. He is the author of *LabVIEW for Electric Circuits, Machines, Drives and Laboratories* (Upper Saddle River, NJ: Prentice-Hall, 2002).

Dr. Ertugrul serves on the Editorial Advisory Board of the *International Journal of Engineering Education* (IJEE).